

Decadal summer drought frequency in China: the increasing influence of the Atlantic Multi-decadal Oscillation

Chengcheng Qian^{1,2}, Jin-Yi Yu¹ and Ge Chen²

¹Department of Earth System Science, University of California, Irvine, CA, USA

²Qingdao Collaborative Innovation Center of Marine Science and Technology, College of Information Science and Technology, Ocean University of China, Qingdao, People's Republic of China

E-mail: jyyu@uci.edu

Received 26 August 2014, revised 24 October 2014

Accepted for publication 10 November 2014

Published 2 December 2014

Abstract

Decadal variations in summer drought events during 1956–2005 are examined over Eastern China to identify their leading variability modes and their linkages to the Pacific Decadal Oscillation (PDO), Atlantic Multi-decadal Oscillation (AMO), and global warming. The PDO influence is found to dominate China drought frequency from the 1960s to early 1990s via modulating the Western Pacific Subtropical High and the Mongolian High. The four-pole drought pattern produced by the PDO diminished after the early 1990s, being replaced by a dipolar drought pattern that is produced by the AMO via a Eurasian wave train emanating from North Atlantic to China. The increasing influence of the AMO on China drought since the early 1990s is further shown to be a consequence of global warming. This study indicates that the early 1990s is a time when the Atlantic began to exert a stronger influence on climate over China and even larger part of Asia.

Keywords: decadal drought frequency in China, Atlantic Multi-decadal Oscillation, global warming, Pacific Decadal Oscillation, early-1990s climate shift, Eurasian wave train

1. Introduction

Frequent drought events have always been a major concern in China due to their pronounced societal and economic impacts (Zou *et al* 2005, Jiang *et al* 2012). The recent 2011 drought, for example, impacted six provinces in the Yangtze River basin, 35 million people, 2 million livestock and 40 million hectare of agricultural area and resulted in a direct economic loss of 15 billion yuan (see <http://www.ce.cn/cysc/ztpd/2011/gh/>). Severe droughts also occurred in northern China in 1997 that resulted in continuous 226 days of no streamflow in the Yellow River (Mishra and Singh 2010). While the observational data is not long enough to determine whether the increased frequency of drought events in recent years is related to human activities (such as the Three-Gorge River

Dam), it is marginally long enough to begin exploring whether decadal fluctuations in the drought occurrences can be linked to any natural global climate variability on decadal or multi-decadal timescales.

Precipitation patterns in Eastern China are known to be characterized by the meridional fluctuation and migration of zonal rain-belts centered over South China, the Yangtze River, the Yellow River, and Northern China (Zhao 1999, Zhou and Yu 2005). This rain-belt feature reflects the dominance of the East Asian monsoon in determining summer precipitation patterns over Eastern China. In association with the monsoon evolution, rain-belts first appear over the southern coast of China in May, move to the Yangtze River region in June, reach northern China in July, and retreat southward in August when the summer monsoon terminates (e.g., Chang *et al* 2000). However, the rain-belt pattern appears to fluctuate decade to decade with noticeable changes suggested to occur in mid-1960s (Yan *et al* 1990), late-1970s (Huang *et al* 1999), early-1990s (Ding and Chan 2005, Kwon



Content from this work may be used under the terms of the Creative Commons Attribution 3.0 licence. Any further distribution of this work must maintain attribution to the author(s) and the title of the work, journal citation and DOI.

et al 2007), or late-1990s (Huang *et al* 2011, Zhu *et al* 2011). The inter-decadal variability has been linked to the Pacific Decadal Oscillation (PDO; e.g., Yang *et al* 2005, Ma 2007, Li *et al* 2010, Qian and Zhou 2014), warming in the tropical Pacific and Indian Oceans (e.g., Hu 1997, Chang *et al* 2000, Yang and Lau 2004, Zhou *et al* 2006, Zhou *et al* 2009, Li *et al* 2010), and human activities (e.g., Menon *et al* 2002, Fu 2003). However, the possible influence from the Atlantic Multi-decadal Oscillation (AMO) has received relatively less attention.

Recent studies have shown that examining the leading patterns of the decadal variations in the drought frequency is one useful way to unveil the underlying causes of changes in drought occurrence (e.g., Zhang 2003, McCabe *et al* 2004). McCabe *et al* (2004) used the lowest quartile (25%) of annual precipitation to define drought events for each of the 344 climate divisions in the conterminous United States, and then calculated the decadal variations in the drought frequency for each region. They were able to use the leading modes of the decadal frequency variations to nicely quantify the individual contributions of the PDO, the AMO, and global warming to the US drought variations in the 20th century. In this study, a similar approach is used to identify the spatial and temporal characteristics of summer drought in Eastern China and their linkages to PDO, AMO, and global warming.

2. Datasets

The data used for the analysis are the monthly precipitation values from the Global Precipitation Climatology Center (GPCC) version 6 covering 1901–2010. In this study, we only focus on the data from 1951 to 2010 because more stations (about 67 200 stations globally) were used for the data set, which makes the record more reliable (Beck *et al* 2005). The NCEP/NCAR reanalysis product is used to provide monthly values for the analysis of surface air temperature (SAT), 1000–300 hPa geopotential height (GHT) and 850 hPa wind vector. The data is available on regular $2.5^{\circ} \times 2.5^{\circ}$ grids from January 1948 to present. Monthly values of the PDO index and the AMO index are used to represent the strengths of these two major decadal variability modes. The PDO index is downloaded from the University of Washington (ftp://ftp.atmos.washington.edu/mantua/pnw_impacts/INDICES/PDO.latest), and the AMO index is downloaded from Earth System Research Laboratory (<http://www.esrl.noaa.gov/psd/data/correlation/amon.sm.data>). The annual-mean Northern Hemispheric surface temperature values are also used in the study and are downloaded from Climate Research Unit (www.cru.uea.ac.uk/cru/data/temperature). The calculation method of these hemispheric temperature means is detailed in Jones *et al* (2012). In this study, the 10-year running means of the Northern Hemisphere temperature values are used to represent the global warming trend and are referred to as the Northern Hemispheric temperature index. In the present study, only the summer (June–July–August; JJA) values of all data from 1956 to 2005 are analyzed, except the Northern hemisphere temperature index whose annual-mean values are

used. Anomalies are defined as the deviations from the corresponding climatological values.

The summer decadal drought frequency (DDF) for Eastern China is calculated from 1956 to 2005 in the same way described in McCabe *et al* (2004), except that a shorter 10-year moving window is used to calculate the frequency. The lowest quartile (25%) of precipitation in 1956–2005 at each grid point is used to define the drought events, and then we calculated the number of drought events happened in the 10-year window. The threshold values (i.e., the lowest 25% of local precipitation) used to define drought events vary from grid points to grid points and are found (not shown) to have the highest precipitation values in the southeast China and decrease from the south to the north and from the coast to inland. We also calculated the DDF using threshold values based on the lowest 30% and 20% of precipitation in the 50-year analysis period and obtained similar patterns. We explored 20-year and 30-year moving windows and find that the DDF pattern is similar to that using the 10-year moving window.

3. Results

3.1. Leading variability modes

We applied an Empirical Orthogonal Function (EOF) analysis to the 1956–2005 variations in the DDF to identify their leading variability modes. The first EOF mode (EOF1; figure 1(a)) exhibits a simple dipolar pattern that describes an out-of-phase relation between the drought variations south and north of the Yellow River. This mode explains 37.22% of the DDF variability. The second EOF mode (EOF2; figure 1(b)) exhibits a more complex four-pole pattern with the DDF anomalies alternating in sign in the Pearl River region (centering at 25°N), the Yangtze River region (centering at 30°N), the Yellow River region (between 35°N and 45°N), and Northeastern China (north of 45°N). This mode explains 23.23% of the DDF variability. It is important to mention that the well-known 'north drought-south flood' pattern of China summer precipitation (e.g., Huang *et al* 2011), which describes the anomalous drought condition in the Yellow River region and an out-of-phase variation in the Yangtze River region, is embedded in this EOF pattern.

To examine the relative importance of the EOF1 and EOF2 modes of the DDF in influencing the summer drought variations, we calculated separately the pattern correlations between the EOF1 and EOF2 patterns and summer DDF patterns from 1956 to 2005. As shown in figure 2, these two EOF modes dominate during different parts of the analysis period. The correlation with EOF1 (red line) stands out from the 95% significance interval (indicated by the shading area) before mid-1960s and after early-1990s, while the correlation with EOF2 (blue line) is the largest during 1960–1990s. The significance interval is determined by a student-t test, which indicates the threshold values for the correlation coefficient to be statistically significant. Therefore, the leading factor that controls China drought frequency is the EOF1 pattern before

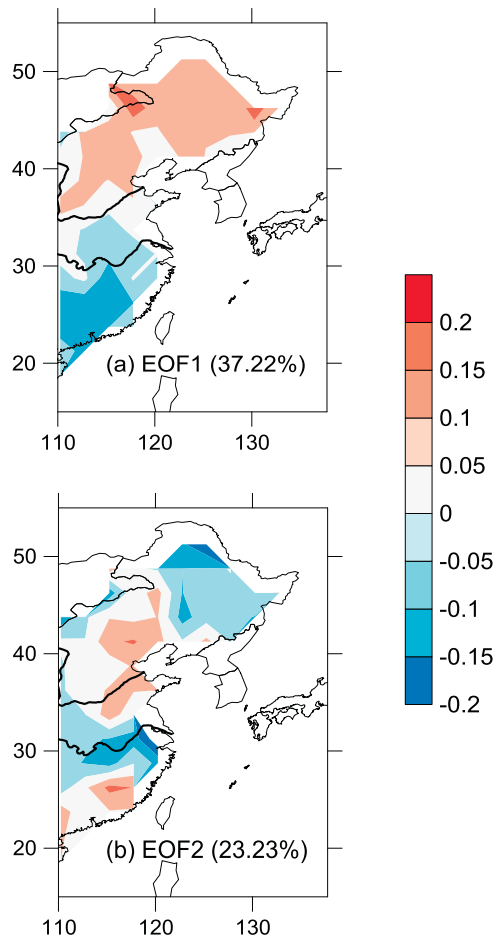


Figure 1. The first two leading EOF modes of summer DDF variations calculated from GPCC dataset (a),(b). Also shown in the figures is the percentage of variance explained by that mode.

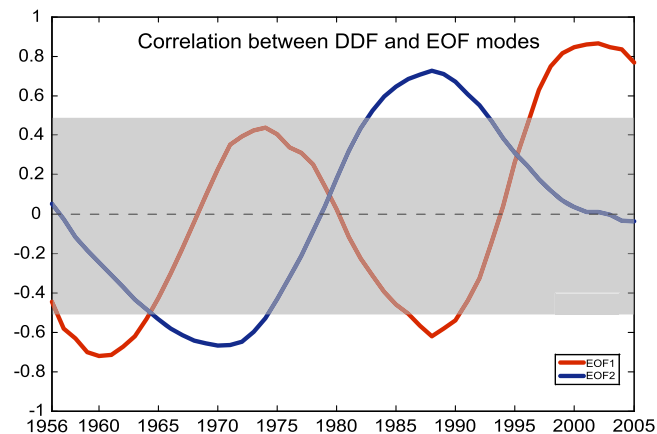


Figure 2. Pattern coefficients between summer DDF patterns in 1956–2005 and EOF1 (red) and EOF2 (blue). The shaded area represents the 95% significant interval. Areas outside the shading means statistically significant in term of the correlation.

1960s, the EOF2 pattern from 1960s to early 1990s, and the EOF1 pattern again after early 1990s. We also notice from figure 2 that the importance of EOF1 exhibits an increasing trend on top of a multi-decadal (~20 years) oscillation. Such a trend does not appear in the relative importance of EOF2.

3.2. Linkages to PDO, AMO, and global warming

To link these two EOF modes of DDF variations to the PDO and AMO, we first calculated the correlation coefficients between the summer DDF variations over Eastern China with the summer values of the AMO and PDO indices. It is interesting to see that the correlation pattern with the AMO (figure 3(a)) resembles EOF1 of the DDF, and the correlation pattern with the PDO (figure 3(b)) resembles EOF2. The pattern correlation coefficient is 0.84 between figure 1(a) and figures 3(a) and 0.94 between figure 1(b) and figure 3(b). This analysis indicates that the two leading EOFs of the DDF variations may separately represent the influences of the AMO and PDO on China droughts.

We then compare in figures 3(c) and (d) the time series of AMO and PDO indices and the principal components (PCs) of EOF1 and EOF2 (PC1 and PC2, hereafter) to further examine their temporal linkages. It is obvious that PC2 and the PDO index vary in phase during the analysis period, as both switch their phases near 1960s, middle-1970s, and late-1990s. The temporal correlation coefficient between these two time series is as high as 0.91. Therefore, the EOF2 of the DDF variations apparently represents the PDO influence on summer China droughts. As for PC1, surprisingly, its temporal correlation with the AMO index is rather low (−0.24), despite the high pattern correlation between their associated spatial structures. While the AMO index exhibits a slow variation with phase changes in early-1960s and early-1990s, PC1 shows higher-frequency (close to 20–25 years) variations. Nevertheless, it is interesting to note that there is a trend in PC1, similar to that noticed in figure 2 for the relative importance of EOF1. It is possible that PC1 contains not only the AMO influence but also the influence from global warming.

To explore this possibility, following McCabe *et al* (2004), we use the annual-mean Northern hemisphere temperature to represent the global warming. As shown in figure 4(a), the Northern hemisphere temperature experiences a weak dip in 1960–1970 and trends upward thereafter. The 1960–1970 dip is a well-known cold period worldwide, which caused speculation at that time that the world was heading for an ice age (Houghton 1997). Figure 4(b) shows the correlation pattern between the Northern hemisphere temperature index and the summer DDF variations. The pattern is characterized by out-of-phase DDF variations to the south and north of the Yellow River, very similar to the EOF1 pattern (figure 1(a)) and DDF pattern regressed onto the AMO index (figure 3(a)). It is likely that, due to their similar impact patterns, the AMO influences and the global warming influences on China droughts are mixed into the EOF1 mode of the DDF variations. The time series of PC1 includes not only the multi-decadal oscillation of the AMO but also the trend caused by the global warming. To separate these two influences in PC1, we first regress PC1 onto the AMO index and then remove this regression from PC1 to produce a ‘PC1-residual’ time series. We find that this residual time series has a high temporal correlation (0.73) with the Northern hemisphere temperature index. We also calculated another ‘PC1-

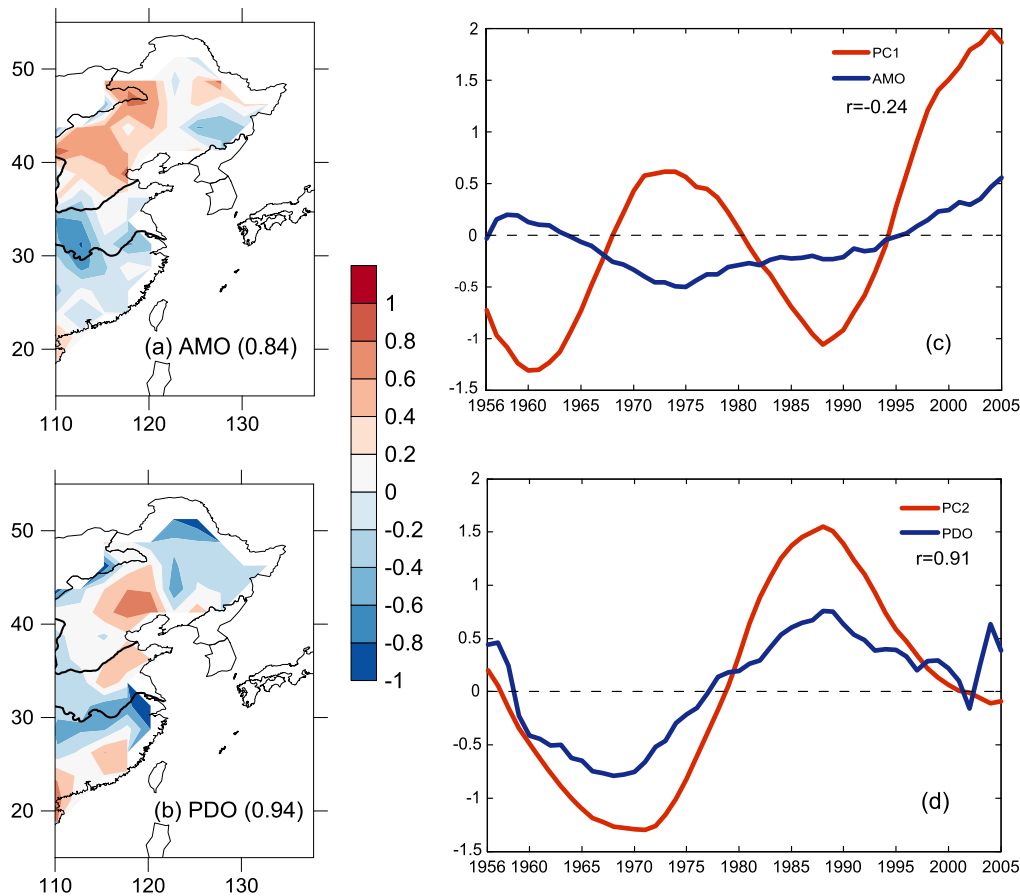


Figure 3. The correlation patterns are shown between the summer DDF variations and the AMO index (a) and the PDO index (b). The correlation coefficients between figure 1(a) and figure 3(a), and figure 1(b) and figure 3(b) are also shown. (c) is the time series of PC1 (red) and AMO index (blue), and (d) is the time series of PC2 (red) and PDO index (blue). The correlation coefficient between each pair of the time series is also shown.

residual’ time series with the regression of PC1 to the Northern Hemisphere temperature index removed. The correlation coefficient is 0.74 between this second ‘PC1-residual’ time series and the AMO index. This is evidence that PC1 represents both the temporal variations of the AMO and global warming influences.

In figure 5, we reconstruct the temporal variations of the zonal-mean DDF anomalies from southern to northern China due to the variation of the AMO index (figure 5(a)) and the Northern hemisphere temperature index (figure 5(b)). The reconstructions are produced as the product of the time series of the index and its corresponding correlation pattern with the DDF variation. The zonal means are calculated as the area-weighted means eastward from 110°E to the coast of Eastern China. Figures 5(a) and (b) show that, despite slightly different locations of the anomaly centers, both the reconstructed DDF variations have a common nodal point at the Yellow River (near 35°N). The drought condition to the north of the River tends to be out-of-phase with the drought condition to the south of the River. The phase variation of AMO causes the Eastern China drought pattern to reverse its polarity to the north and south of the Yellow River around 1960s and 1990s. As for global warming, it causes the drought pattern to reverse its polarity to the north and south of the Yellow River

around 1980. Combining both the AMO and global warming contributions (figure 5(c)), the out-of-phase drought condition to the north and south of the Yellow River reverses its polarity in early-1960s, early-1980s, and 1990s. The combined variations are close to the variations reconstructed based on PC1 and EOF1 (figure 5(d)) before the mid-1960s and after the 1990s. Additionally, both show a tendency to vary on bi-decadal timescales. Therefore, the bi-decadal variability revealed by EOF1 for summer China droughts results from the combined influences of AMO and global warming. Figure 5(c) also reveals that the AMO and global warming influences tended to cancel out each other in 1960–1990s. After early-1990s, the AMO and global warming influences were in phase and their combined influence identifies and dominates the summer drought pattern in Eastern China.

By conducting a similar reconstruction using PC2 and EOF2, we notice from figure 5(e) that the four-pole drought pattern in Eastern China reversed its polarity in late-1970s when the PDO changed its phase. Combining together the reconstruction patterns from PC1 and PC2 (figure 5(f)), we pretty much recover the DDF variations observed during the analysis period (figure 5(g)). According to figures 5(f) and (g), the characteristics of China drought pattern divide the

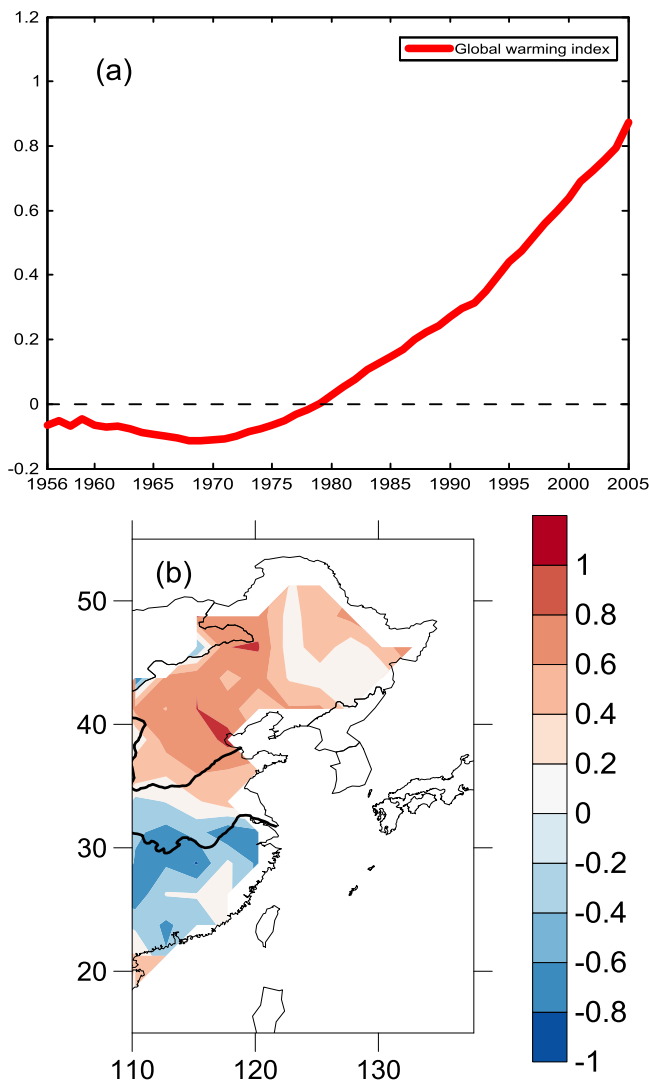


Figure 4. (a) The time series of Northern Hemisphere temperature index and (b) its correlation pattern with the summer DDF variations.

analysis period into three sub-periods: before early-1960s, from 1960s to early-1990s, and after early-1990s. The negative phase of the EOF1 pattern dominated the drought pattern before early-1960s, and this drought pattern is contributed primarily by the cooling dip in the Northern hemisphere temperature index (see figures 5(b) and (g)). For the second period from early-1960s to early-1990s, the China drought pattern is determined by the EOF2 pattern that represents the PDO influence. The four-pole pattern and its phase reversal in late-1970s dictates China drought occurrence in summer. However, this PDO control diminishes after early-1990s and gives way to the dipolar pattern of the EOF1. In contrast to the EOF1 control before early-1960s, the EOF1 control after early-1990s is related to the re-enhancement of the AMO and global warming influences. As shown in figures 5(a) and (b), the DDF variations caused by the AMO and global warming are in-phase during this period. In conclusion, we find the summer drought conditions over Eastern China to be dominated by global warming (actually ‘cooling’) influences

before 1960s, by the PDO from 1960s to 1990s, and recently (after early 1990s) by the AMO under global warming.

3.3. The linking mechanisms

To understand the mechanism that links the dipole drought pattern of EOF1 to the AMO, we contrast atmospheric patterns regressed onto PC1 and the AMO index. As shown in figure 6(a), the SAT anomalies regressed to PC1 are dominated by a warming over the North Atlantic Ocean. This regression pattern is close to the SAT anomaly pattern regressed to the AMO index (figure 6(b)), both of which reflect the typical SST anomaly pattern associated with the AMO (e.g., Enfield *et al* 2001, Knight *et al* 2005, Sutton and Hodson 2005). This similarity indicates that EOF1 is indeed related to the AMO. The mechanism that enables the AMO to impact China can be revealed by looking into the vertically-integrated (1000–300 hPa) GHT anomalies regressed to the AMO index (figure 6(d)). The figure shows that a wavetrain emerges over the Euro-Asia sector, which includes an anti-cyclonic anomaly center over the North Atlantic, a cyclonic anomaly center over the Ural mountain region and an anti-cyclonic anomaly center over the Mongolia Plateau and Northern China. The GHT regression to PC1 reveals a similar pattern (figure 6(c)). This wavetrain pattern is similar to the Eurasia (EU) pattern of teleconnection identified by Wallace and Gutzler (1981) over the North Atlantic and Eurasia. It should be noted that there are several variants of this so-called EU teleconnection pattern: including that identified by Liu *et al* (2014) as the conventional EU pattern and those identified by Barnston and Livezey (1987) as the EU pattern type 1 (EU1; or Scandinavia pattern) and EU pattern type 2 (EU2; or East Atlantic/West Russia pattern). The pattern we identified in figure 6(c) is closest to the conventional EU pattern discussed by Liu *et al* (2014). As part of this pattern, an anti-cyclonic anomaly center is established to the north of the Yellow River while a cyclonic anomaly center established to the south of the Yellow River. The southern cyclonic center produces southerly anomalies over Eastern China to enhance the summer monsoon and brings more precipitation to the region south of the Yellow River. Conversely, the northern anti-cyclonic center produces northerly anomalies to weaken the summer monsoon and reduce precipitation to the region north of the Yellow River. Consequently, drought conditions exist to the north of the Yellow River, while flood conditions exist to the south of the River. A modeling study by Wang *et al* (2009) also showed that a positive phase of the AMO can cause above-normal summer rainfall in the southeastern part of China, which is consistent with the flood condition we report here south of the Yellow River. Also, the EU pattern we describe here is similar to the ‘Silk Road’ teleconnection pattern identified by Huang *et al* (2012) that spans the entire Asian continent to modulate the strength of East Asian Monsoon. Therefore, the dipolar drought pattern of EOF1 is linked to the AMO via an EU wavetrain emanating from the North Atlantic.

The SAT variation pattern regressed to PC2 (figure 6(e)) is close to the regression pattern to the PDO index

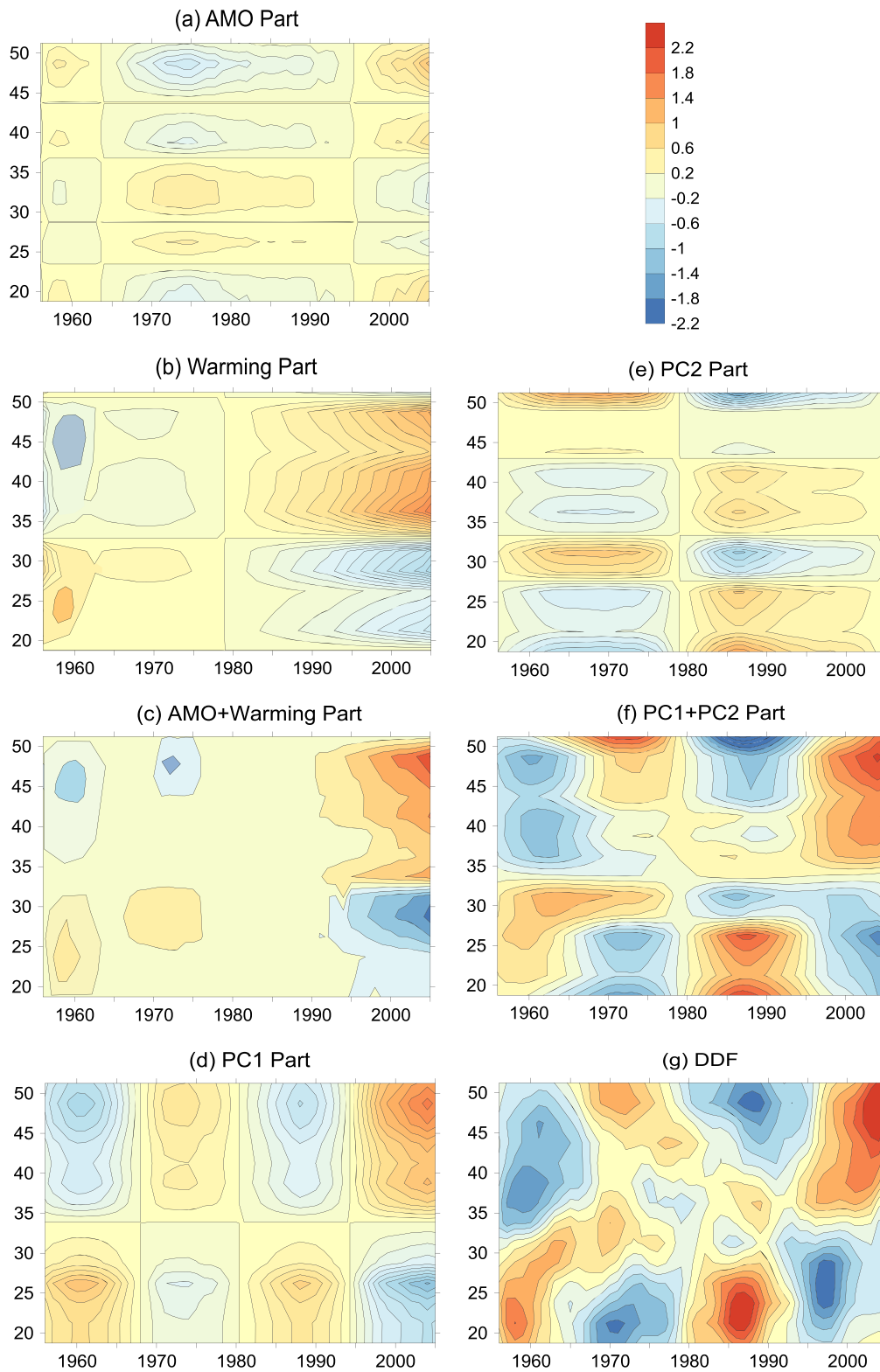


Figure 5. Reconstruction of the summer DDF variations in East China based on (a) the AMO index, (b) the Northern Hemisphere temperature index, (d) the PC1, and (e) the PC2. The summation of (a) and (b) are shown in (c). The summation of (d) and (e) are shown in (f). The zonally-averaged DDF variations are shown in (g). The values shown are the DDF variations zonally averaged in China eastward from 110° E. The numbers in the color bar represent the number of drought (positive values) or flood (negative values) events per decade.

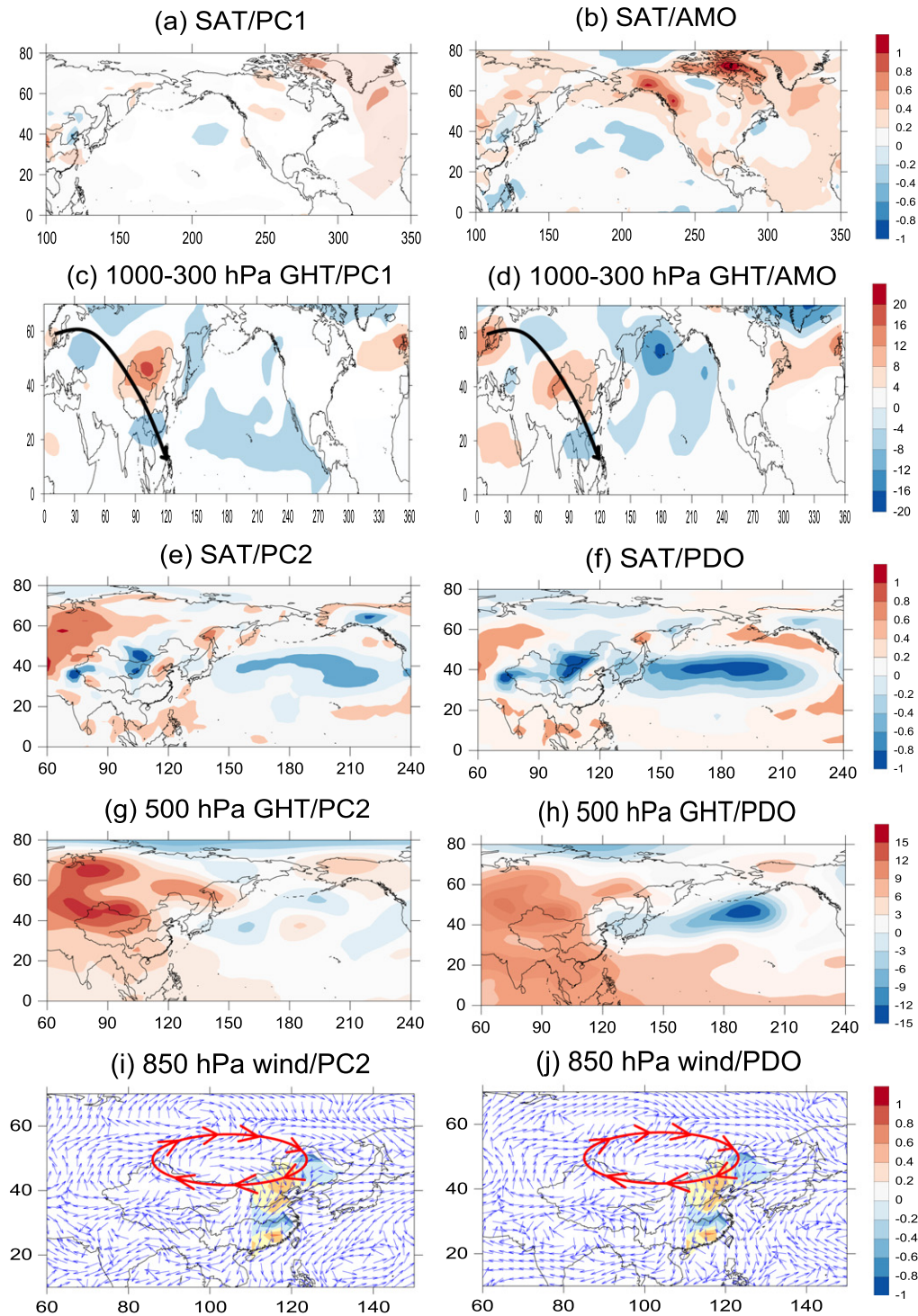


Figure 6. The regression of surface air temperature (a),(b) and geopotential height integrated from 300 to 1000 hPa (c),(d) to PC1 (left panels) and AMO index (right panels). The regression of surface air temperature (e),(f), 500 hPa geopotential height (g),(h), and 850 hPa wind vectors (i),(j) with PC2 (left panels) and PDO index (right panels). The DDF pattern of EOF2 (color shading) is also shown in (i) and (j).

(figure 6(f)), both of which reflect the typical SST anomaly pattern of the PDO that is characterized by positive SAT anomalies over the tropical east Pacific and negative SAT anomalies over the north Pacific (Mantua *et al* 1997). Therefore, the four-pole drought pattern of EOF2 is related to the PDO. The two southern poles (indicated by the color shading in the figures) centered over the Pearl River region

and the Yangtze River region can be explained by a southward displacement of the western Pacific subtropical high (WPSH) induced by the PDO, as revealed in figures 6(g) and (h) where the 500 hPa GHT anomalies are regressed to PC2 and the PDO index respectively. The two patterns are very similar and both show a southward displacement of the WPSH with negative GHT anomalies over the western Pacific

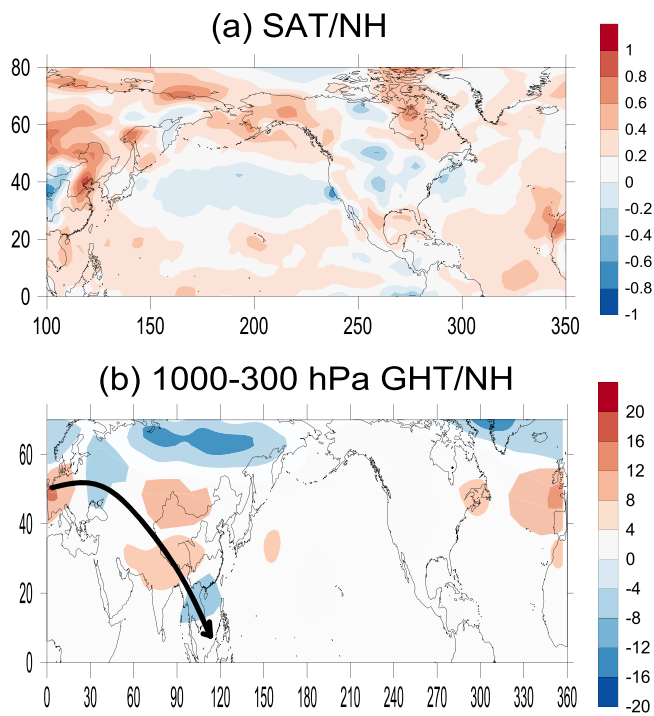


Figure 7. The regression of the anomalies of (a) surface air temperature and (b) geopotential height integrated from 300 to 1000 hPa (b) onto the Northern Hemisphere temperature index.

along 30°–40°N and positive anomalies over southern China. This displacement results in drought conditions in the Pearl River region via sinking airflow and relieves the drought conditions over the Yangtze River region. The northern two poles of EOF2 can be explained as a result of the PDO-induced enhancement of the Mongolian High. Figures 6(i) and (j) show the regression of 850 hPa wind vector with PC2 and the PDO index. Again, both patterns are similar and reveal a strong anomalous anticyclone centered over the Mongolia Plateau. This wind pattern enhances the westerly jet on its polar flank increasing the moisture transport toward Northeast China to reduce drought occurrence. The same anticyclonic anomaly weakens the westerlies in its southern flank decreasing the moisture transport into the Yellow River region to enhance drought occurrence. As a result, the northern two poles of the EOF2 pattern are established. Therefore, the PDO induces the four-pole drought pattern of EOF2 via a modulation of the location of the WPSH and the intensity of the Mongolian High.

We also explored the mechanism that enables the global warming to impact China summer droughts by regressing SAT and vertically-integrated (1000–300 hPa) GHT anomalies onto the Northern Hemisphere index. As shown in figure 7(a), the temperature index is associated with positive SAT anomalies over most of the Northern Hemisphere, except for parts of the mid-latitude Pacific. The regressed GHT anomaly pattern shown in figure 7(b) is not similar to the pattern regressed onto the AMO index (see figure 6(d)). However, both patterns show similar anomalies over East China: positive GHT anomalies to the north of Yellow River and negative GHT anomalies to the South of the Yellow

River. This similarity explains why both the AMO and global warming have similar impacts on East China drought.

4. Conclusion

This study examined the decadal variations of summer drought events over Eastern China to identify their leading variability modes and their linkages to the PDO, AMO, and global warming. While the PDO used to be the dominant controlling factor, its importance to China summer droughts has diminished since the early 1990s. Since then, the drought patterns in China have been more strongly influenced by the AMO. An Atlantic-EU wavetrain emanating from the North Atlantic enables the AMO to impact China droughts. This study also finds that the increasing importance of the AMO since the early 1990s is a consequence of global warming. A similar positive phase of AMO in the period before 1960s did not produce the same influence on China drought as that observed after the early 1990s. A global ‘cooling’ occurring at that time tended to cancel out the AMO influence. Related to the influence of global warming, the summer drought pattern in China after the early-1990s has entered a new era that is more controlled by the condition in the Atlantic Ocean than by the condition in the Pacific Ocean. Thus, the early-1990s should be regarded as a time when the Atlantic began to exert a strong influence on the climate over China and even other regions of East Asia and the Western Pacific. This finding is consistent with the findings of Yu *et al* (2014) that suggested the AMO is a possible cause for the shift in the location of El Nino from eastern Pacific to central Pacific since the early 1990s. Our findings on the change in the China drought patterns and their linkage to the Atlantic have important implications on how to further improve climate predictions in the region.

Acknowledgments

This research is supported by US National Science Foundation Grant AGS-1233542 and NOAA Grant NA11OAR4310102, the Natural High Technology Program of China under Projects 2013AA09A505 and SS2013AA12120303, and the Basic Scientific Research Operating Expenses of Ocean University of China. Chengcheng Qian is a visiting student at University of California, Irvine from Ocean University of China.

References

Barnston A G and Livezey R E 1987 Classification, seasonality and persistence of low-frequency atmospheric circulation patterns *Mon. Weather Rev.* **115** 1083–126
 Beck C, Grieser J and Rudolf B 2005 A new monthly precipitation climatology for the global land area for the period 1951–2000 *Geophys. Res. Abstr.* **7** 07154

- Chang C, Zhang Y and Li T 2000 Interannual and interdecadal variations of the East Asian summer monsoon and tropical Pacific SSTs. Part I: roles of the subtropical ridge *J. Clim.* **13** 4310–25
- Ding Y H and Chan J C L 2005 The East Asian summer monsoon: an overview *Meteorol. Atmos. Phys.* **89** 117–42
- Enfield D B, Mestas-Nuñez A M and Trimble P J 2001 The Atlantic Multidecadal Oscillation and its relation to rainfall and river flows in the continental US *Geophys. Res. Lett.* **28** 2077–80
- Fu C B 2003 Potential impacts of human induced land cover change on East Asia monsoon *Glob. Planet. Change* **37** 219–29
- Ge Q, Dai J, He F, Zheng J, Man Z and Zhao Y 2004 Spatiotemporal dynamics of reclamation and cultivation and its driving factors in parts of China during the last three centuries *Prog. Nat. Sci.* **14** 605–13
- Houghton J 1997 *Global Warming: The Complete Briefing* (Cambridge: Cambridge University Press) p 7
- Hu Z 1997 Interdecadal variability of summer climate over East Asia and its association with 500 hPa height and global sea surface temperature *J. Geophys. Res.* **102** 19403–12
- Huang R H, Xu Y H and Zhou L T 1999 The interdecadal variation of summer precipitations in China and the drought trend in North China *Plateau Meteor.* **18** 465–76 (in Chinese)
- Huang R H, Chen J L, Lin W and Lin Z 2012 Characteristics, processes, and causes of the spatio-temporal variabilities of the East Asian monsoon system *Adv. Atmos. Sci.* **29** 910–42
- Huang R H, Chen J L and Liu Y 2011 Interdecadal variation of the leading modes of summertime precipitation anomalies over Eastern China and its association with water vapor transport over East China *Chin. J. Atmos. Sci.* **35** 589–606 (in Chinese)
- Jiang Z, Song J, Li L, Chen W, Wang Z and Wang J 2012 Extreme climate events in China: IPCC-AR4 model evaluation and projection *Clim. Change* **110** 385–401
- Jones P D, Lister D H, Osborn T J, Harpham C, Salmon M and Morice C P 2012 Hemispheric and large-scale land surface air temperature variations: an extensive revision and an update to 2010 *J. Geophys. Res.* **117** D05127
- Knight J R, Allan R J, Folland C K, Vellinga M and Mann M E 2005 A signature of persistent natural thermohaline circulation cycles in observed climate *Geophys. Res. Lett.* **32** L20708
- Kwon M H, Jhun J G and Ha K J 2007 Decadal change in East Asian summer monsoon circulation in the mid-1990s *Geophys. Res. Lett.* **34** L21706
- Li H, Dai A, Zhou T and Lu J 2010 Responses of East Asian summer monsoon to historical SST and atmospheric forcing during 1950–2000 *Clim. Dyn.* **34** 501–14
- Liu Y, Wang L, Zhou W and Chen W 2014 Three Eurasian teleconnection patterns: spatial structures, temporal variability, and associated winter climate anomalies *Clim. Dyn.* **42** 2817–39
- Ma Z 2007 The interdecadal trend and shift of dry/wet over the central part of north China and their relationship to the Pacific Decadal Oscillation (PDO) *Chin. Sci. Bull.* **52** 2130–9
- Mantua N J, Hare S R, Zhang Y, Wallace J M and Francis R C 1997 A Pacific interdecadal climate oscillation with impacts on salmon production *Bull. Am. Meteorol. Soc.* **78** 1069–79
- McCabe G J, Palecki M A and Betancourt J L 2004 Pacific and Atlantic Ocean influences on multidecadal drought frequency in the United States *Proc. Natl Acad. Sci.* **101** 4136–41
- Menon S, Hansen J, Nazarenko L and Luo Y 2002 Climate effects of black carbon aerosols in China and India *Science* **297** 2250–3
- Mishra A K and Singh V P 2010 A review of drought concepts *J. Hydrol.* **391** 202–16
- Qian C and Zhou T 2014 Multidecadal variability of north China aridity and its relationship to PDO during 1900–2010 *J. Clim.* **27** 1210–22
- Sutton R T and Hodson D L R 2005 Atlantic Ocean forcing of north American and European summer climate *Science* **309** 115–8
- Wallace J M and Gutzler D S 1981 Teleconnections in the geopotential height field during the Northern hemisphere winter *Mon. Weather Rev.* **109** 784–812
- Wang Y, Li S and Luo D 2009 Seasonal response of Asian monsoonal climate to the Atlantic multidecadal Oscillation *J. Geophys. Res.* **114** D02112
- Yan Z, Ji J and Ye D 1990 Northern hemispheric summer climatic jump in the 1960s: I. Precipitation and temperature *Sci. China Ser. B* **33** 97–103
- Yang F and Lau K 2004 Trend and variability of China precipitation in spring and summer: linkage to sea-surface temperatures *Int. J. Climatol.* **24** 1625–44
- Yang X Q, Xie Q, Zhu Y M, Sun X G and Guo Y J 2005 Decadal to interdecadal variability of precipitation in north China and associated atmospheric and oceanic anomaly patterns (in Chinese) *Chin. J. Geophys.* **48** 789–97
- Yu J-Y, Kao P-K, Paek H, Hsu H-H, Hung C-W, Lu M-M and An S-I 2014 Linking emergence of the Central-Pacific El Niño to the Atlantic Multi-decadal Oscillation *J. Clim.* in press doi:10.1175/JCLI-D-14-00347.1
- Zhang Q 2003 *Droughts and its Impacts, in China Climate Impact Assessment* ed H Chen (Beijing: Meteorological Press) pp 12–5
- Zhao Z G 1999 *Summertime Floods and Droughts in China and the Associated Circulations* (in Chinese) (Beijing: Meteorological Press)
- Zhou T J and Yu R C 2005 Atmospheric water vapor transport associated with typical anomalous summer rainfall patterns in China *J. Geophys. Res.* **110** D08104
- Zhou T et al 2009 Why the western Pacific subtropical high has extended westward since the late 1970s *J. Clim.* **22** 2199–215
- Zhou W, Li C Y and Chan J C L 2006 The interdecadal variations of the summer monsoon rainfall over south China *Meteorol. Atmos. Phys.* **93** 165–75
- Zou X, Zhai P and Zhang Q 2005 Variations in droughts over China: 1951–2003 *Geophys. Res. Lett.* **32** L04707
- Zhu Y, Wang W, Zhou W and Ma J 2011 Recent changes in the summer precipitation patterns in East China and the background circulation *Clim. Dyn.* **36** 1463–73